

GMAW 短路过渡过程中瞬时短路现象的分析

王广伟, 蔡 艳, 华学明, 吴毅雄

(上海交通大学 焊接工程研究所, 上海 200030)

摘 要: 对 GMAW 短路过渡过程中的瞬时短路现象进行了力学动态分析, 建立了基于熔滴液体压力、电磁收缩力、表面张力的瞬时短路力动态平衡临界条件。通过微距高速摄影技术和图像处理技术, 获得了熔滴半径的变化数据, 并结合电信号分析。结果表明, 计算所得数值所反映的短路进程状态和图像所示的完全吻合, 认为瞬时短路力动态平衡临界条件真实有效。并进一步基于此临界条件分析了熔滴形态对瞬时短路的影响, 认为熔滴和熔池接触瞬间的径向半径如果小于轴向半径, 则接触处的径向表面张力所产生的压力大于零, 瞬时短路开始且不可逆, 即纺锤形熔滴易造成瞬时短路。最后对瞬时短路现象进行了分类和定量研究, 并提出了瞬时短路现象的新的解释。

关键词: 力动态平衡; 瞬时短路; 熔化极气体保护焊

中图分类号: TG434 **文献标识码:** A **文章编号:** 0253-360X(2007)09-043-05



王广伟

0 序 言

熔化极气体保护焊(GMAW)中的金属过渡是通过焊丝熔化形成熔滴再过渡到母材的形式进行的, 熔滴过渡过程决定了整个焊接过程稳定性的好坏以及最终焊接质量的优劣。根据不同的焊接工艺实现熔滴过渡的方式有: 大滴过渡, 射流过渡和短路过渡。其中短路过渡过程一直存在两大问题没有很好地解决: 存在较大的飞溅; 焊缝质量和成形不好。而其中瞬时短路现象(以下简称瞬短), 是造成这两大问题的重要原因, 因此对瞬短现象及机理进行研究很有意义。

瞬短现象以往多局限于定性分析, 被定义为: 电极在非常短的时间和熔池发生接触, 但没有发生金属过渡^[1-3]。较早些时候的解释为^[4]: 液态的熔滴金属和熔池金属一旦发生接触, 原来分布于焊丝表面较大区域的焊接电流将全部集中于接触点形成短路电流, 使接触点电流密度增大, 造成局部过热汽化蒸发, 结果很快脱离接触, 造成瞬时短路。如果熔滴是在较大的电流下与熔池发生短路接触, 而且短路之后电流立即以较快速度上升, 电流产生较大的电磁力会阻止熔滴金属向熔池过渡, 严重时会在熔滴金属与熔池之间的接触面上形成缩颈, 发生电爆炸, 使大部分熔滴金属被抛出, 造成瞬时短路飞溅。从

短路时间进行分析, 根据试验可以认为短路过渡存在两种短路形式: 一种持续时间较长, 约为 $(7 \sim 8) \times 10^{-3}$ s 为 A 型短路; 另一种持续时间较短, 约为 $(0 \sim 1) \times 10^{-3}$ s 为 B 型短路。通常把 B 型短路认为是瞬短^[4]。

在之前对瞬短现象的研究中, 没有考虑熔滴形态的影响和力学条件的动态变化。作者研究基于微距高速摄像技术, 对熔化极气体保护焊短路过渡过程中存在的瞬短现象进行分类研究和定量分析, 进一步阐明瞬短现象的机理。

1 瞬时短路发生的力动态平衡临界条件

1.1 力动态平衡分析

熔滴和工件表面相互接触时, 熔滴和熔池表面接触示意图如图 1 所示。初始缩颈位置发生在接触位置 A 点附近, 此缩颈位置受到三个主要的压力: 熔滴液体压力、电磁收缩力、表面张力。根据电磁学和流体力学理论, 下式分别为液态熔滴与熔池表面接触中心位置所受的液体压力、电磁收缩力、表面张力的径向压力, 由于均作用于液体上因此需用压强来表示。液态熔滴与熔池接触处产生的液体压力为

$$p_l(t) = h(t)g\rho_{liq} \quad (1)$$

式中: ρ_{liq} 为熔滴的密度; $h(t)$ 为整个熔滴轴向上的长度。

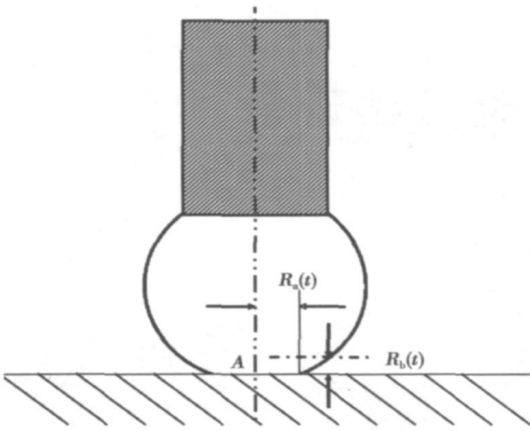


图 1 瞬时短路接触示意图

Fig. 1 Schematic drawing for short circuit contact

推导位置 A 处所受的电磁收缩压力,以图 2 的 A 位置径向截面导体为研究对象,设截面半径为 R , 电流为 I 。

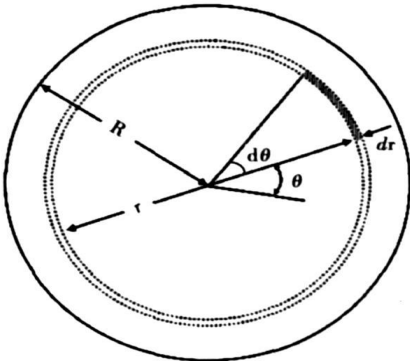


图 2 A 位置径向截面

Fig. 2 Radial section of A point

则在半径为 r 的圆周上的所有点的电磁力方向均指向导体内侧,所以对导体内侧产生径向压力 (p),其单元增量为

$$-dp = \frac{df}{rd\theta} = 2 \frac{r}{R^2} I \cdot \frac{dr}{\pi R^2} I. \quad (2)$$

$$p = \int_R^r dp = \frac{I^2}{\pi R^4} (R^2 - r^2). \quad (3)$$

由于 A 处为液态,因此压力将产生轴向压力,总压力为

$$p_{\text{总}} = \frac{\mu_0}{4\pi} \int_0^R p 2\pi r dr = \frac{\mu_0}{8\pi} I^2. \quad (4)$$

因此 A 点位置所受的径向电磁压力为

$$p_r(t) = \frac{F}{\pi R_a^2(t)} = \frac{\mu_0 I^2(t)}{8\pi^2 R_a^2(t)}, \quad (5)$$

式中: μ_0 为真空磁导率; $R_a(t)$ 为液桥 A 点附近径切后曲线的曲率半径; $I(t)$ 为接触处的通过电流。

液态熔滴与熔池接触处的径向表面张力所产生的压力为

$$p_s(t) = \sigma \left[\frac{1}{R_a(t)} - \frac{1}{R_b(t)} \right], \quad (6)$$

式中: σ 为表面张力; $R_a(t)$ 液桥 A 点附近径切后曲线的曲率半径; $R_b(t)$ 液桥 A 点附近轴切后曲线的曲率半径。

1.2 力动态平衡临界条件

在短路瞬间,熔滴与熔池相交侧表面处的夹角不同,造成 $R_a(t)$, $R_b(t)$ 的值变化很大,表面压力 $p_s(t)$ 因此出现正值或者负值,正的表面压力表明表面压力的方向径向内指,阻碍熔滴的铺展;负的表面压力表明表面压力的方向径向外指,对熔滴的铺展有利。

综合考虑熔滴液体压力、电磁收缩力、表面张力所产生的压力,若接触处的内指径向总压力大于轴向向下总压力时,在图 1 的 A 点位置处将发生收缩直至破断,造成瞬时短路。因此,发生瞬时短路的力动态平衡临界条件为

$$p_s(t) + p_r(t) > p_l(t). \quad (7)$$

即

$$\sigma \left[\frac{1}{R_a(t)} - \frac{1}{R_b(t)} \right] + \frac{\mu_0 I^2(t)}{8\pi^2 R_a^2(t)} > h(t) g \rho_{\text{liq}}. \quad (8)$$

2 瞬短形态研究

2.1 熔滴形状的动态变化

燃弧期随着焊丝的熔化,熔滴的体积逐渐增大,熔滴形状的动态变化直接影响熔滴的轴向长度变化和熔滴下端的形状,因此熔滴的形态对瞬短是否发生是关键因素之一。

不考虑电磁力和斑点力的情况下,熔滴较小时,重力作用不明显,熔滴上的主要作用力为表面张力,表面张力的作用使液体的表面能降到最小,自由液滴则总是趋于球形,凸液面的压力指向球心内侧,因此,在熔滴比较小时,表面张力起到阻碍熔滴过渡的作用,并维持熔滴呈球形^[5,6];熔滴较大时,由于重力的作用将轴向拉长熔滴,呈椭圆或下垂形^[7,8]。

考虑电磁力和斑点力的情况下,对熔滴的作用取决于弧根和熔滴的大小。熔滴较小时,熔滴上的轴向电磁分力向上,对熔滴起支撑作用,克服重力的作用,维持熔滴呈球形;熔滴较大时,燃弧段后期弧根扩展,轴向电磁力向下,使熔滴有拉长的趋势,而

斑点力则对熔滴起支撑作用。

2.2 试验及分析

基于微距高速摄影技术以2 000 帧/s的拍摄速度使用 OTC 焊机 DP500,以100 kHz的采样频率对电流电压信号进行同步采样;采用焊接工艺参数为电压20 V,电流 110 A;保护气体为 CO₂+Ar 混合气,流量为 15 L/min;送丝速度为0.035 m/s;对短路过渡过程进行图像分析研究,发现熔滴在燃弧后期呈现纺锤形时,熔滴尖端接触熔池易发生瞬短,如图3~图7所示。

分别对过程 I, II, III, IV 和正常短路过程进行力动态平衡定量分析,令

$$p'(t) = p_r(t) + p_s(t) - p_l(t),$$
结果如表 1 所示。

表 1 不同过程的受力分析						
Table 1 Analysis of forces in different processes						
过 程 I						
图 像 号	电 流 $I(t)$ /A	径向 半径 $R_a(t)$ /(10 ⁻⁴ m)	液体 压力 $p_l(t)$ /(N·m ⁻²)	径向电 磁压力 $p_r(t)$ /(N·m ⁻²)	表面 压力 $p_s(t)$ /(N·m ⁻²)	合压力 $p'(t)$ /(N·m ⁻²)
2	95.2	2.3	50.9	2 611.2	-2 705.5	-43.4
3	100.4	3.0	51.6	1 732.9	-993.4	687.9
4	125.2	2.8	49.1	3 123.8	960.3	4 035.0
5	162.3	1.8	44.8	12 700.0	2 727.2	15 382.4
过 程 II						
3	118.4	1.8	40.6	6 414.4	-577.6	5 796.2
4	99.8	1.4	32.1	7 197.5	2 746.8	9 912.2
过 程 III						
3	100.1	1.1	42.5	12 728.1	882.8	13 568.4
过 程 IV						
3	151.2	1.1	40.0	28 855.5	839.3	29 654.8
正常短路过程						
3	59.8	3.3	42.8	525.5	-6 712.8	-6 187.3
4	68.5	5.9	35.9	216.3	-2 013.6	-1 797.3

需要说明的是 OTC — DP500 焊机在短路过渡初期,检测到电压陡降的信号后,将对电流进行一定时间和程度的抑制,防止电流上升过快造成的不稳定现象。根据表 1,过程 I 的电流呈上升趋势,径向半径 $R_a(t)$ 则先增大后减小(液桥出现一定的铺展后缩颈), $p_l(t)$ 因为熔滴形态变化和送丝的综合影响,增大之后减小; $p_r(t)$ 综合考虑 $R_a(t)$ 和 $I(t)$ 则先减小后增大; $p_s(t)$ 和 $p'(t)$ 保持增大的趋势。

过程 II 中,尽管电流略微下降,但是由于 $R_a(t)$ 较小 $p_r(t)$ 依然很大,且随着 $p_s(t)$ 的变化 $p'(t)$ 一直保持着较大的数值并且呈上升趋势。过程 III、IV 由于熔滴和熔池接触后 $p'(t)$ 较大达到 10⁵ 数量级,因此在0.5 ms 的时间内就完成了瞬短的过程。整个

表 1 的数值所反映的短路进程状态和图像所示的完全吻合,因此可以认为瞬短力动态平衡临界条件真实有效。

进一步对临界条件进行讨论,在上述四个过程中, $p_l(t)$ 的数量级为 10² 相对 $p_r(t)$ 小很多,因此只要 $p_s(t)$ 为正值则 $p'(t)$ 就大于零,即满足瞬短力动态平衡临界条件,液桥无法继续铺展发生收缩直至破断,且这一过程不可逆。而 $p_s(t)$ 是否为正,则取决于径向半径 $R_a(t)$ 与轴向半径 $R_b(t)$,因此一般可以认为熔滴形态特别是熔滴下端的形态对是否发生瞬短具有决定意义,这也是纺锤形熔滴较易发生瞬短的原因。

以上四个过程是整个试验中受熔滴形态影响而造成瞬短的两大大类典型过程(过程 I、II 为 A 类过程,过程 III、IV 为 B 类过程)。A 类过程比 B 类过程耗时更多,分别为 1~2 ms 和 0~1 ms,这和 $p'(t)$ 的大小有关。采用图像处理技术,对 A 类过程和 B 类过程熔滴体积变化情况进行定量分析,A 类过程存在金属过渡,过程 I, II 过渡量分别为 5.25×10⁻¹¹ m³ 和 3.55×10⁻¹¹ m³,B 类过程,图像处理技术已无法测算过渡量大小,可以认为其没有建立液桥,没有发生金属过渡。从瞬短力动态平衡临界条件可以看出,不同的工艺条件下,电流波形的不同会对瞬短持续的时间造成很大的影响。因此之前对瞬短的定义“电极在非常短的时间和熔池发生接触,但没有发生金属过渡”是不细致的。建议应该摒弃时间概念,认为类似 B 类过程为瞬时短路过程,定义为:熔化电极和熔池接触但没有形成液桥的短路现象。而把类似 A 类,液桥建立但没有完全铺展开的短路过渡过程定义为瞬时短路过渡(instantaneous short circuit transfer)。

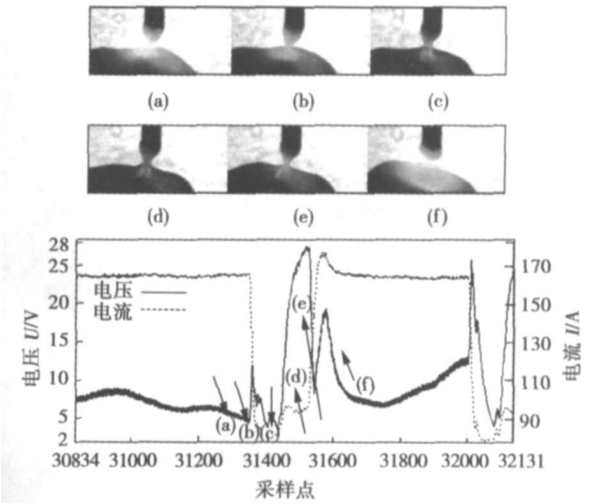


图 3 过程 I 图像与电信号波形图

Fig. 3 Photographs and waveform of process I

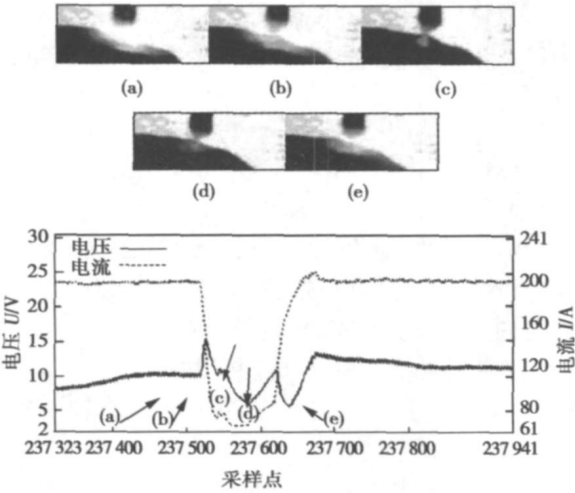


图 4 过程 II 图像与电信号波形图
Fig. 4 Photoraphs and waveform of process II

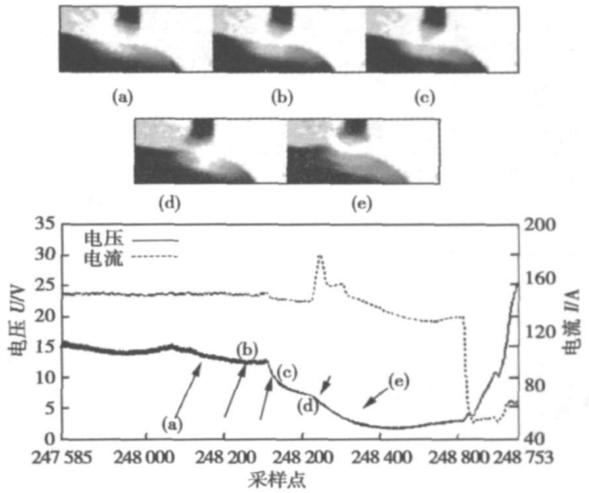


图 5 过程 III 图像与电信号波形图
Fig. 5 Photoraphs and waveform of process III

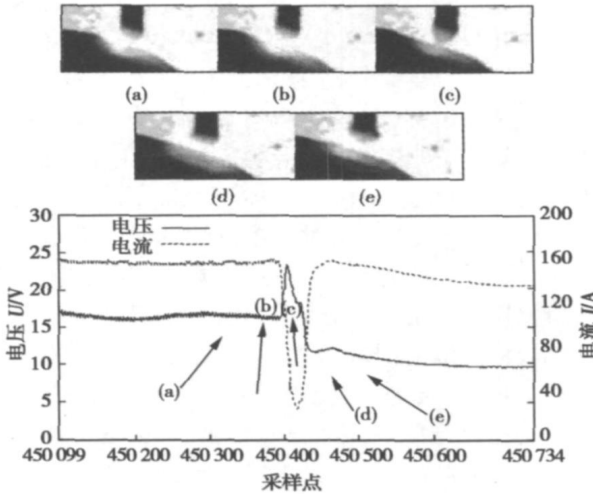


图 6 过程 IV 图像与电信号波形图
Fig. 6 Photoraphs and waveform of process IV

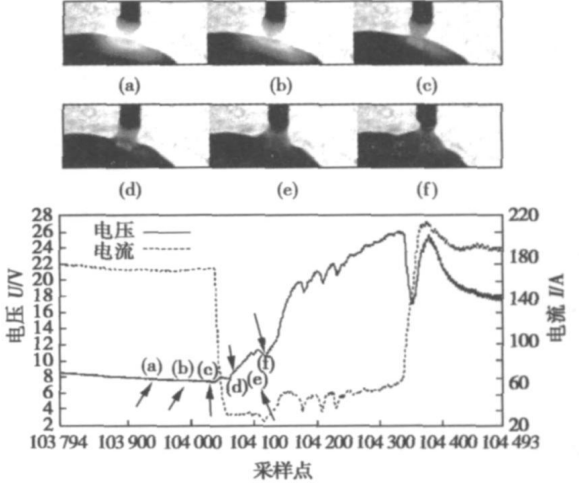


图 7 正常短路过程图像与电信号波形图
Fig. 7 Photoraphs and waveform of normal sht circuiting processes

3 结 论

(1) 建立了瞬短力动态平衡临界条件方程式, 并且通过微距高速摄像图像分析, 结合电信号定量计算, 证明此临界条件能够真实的反应瞬短的进程。

(2) 分析了熔滴形态对瞬短的影响, 并且认为一般情况下熔滴形态特别是熔滴下端的形态对是否发生瞬短具有决定意义。

(3) 基于图像处理技术对瞬短现象进行了分类, 认为 A 类存在少量的金属过渡, 而 B 类则因为 $p'(t)$ 过大, 无法建立液桥而几乎不存在金属过渡, 并以此提出了瞬短现象的新定义。

参考文献:

[1] Cooksey C J, Milner D R. Metal transfer in gas-shielded arc welding [C] // Proc. Symp. Physics of the Welding Arc. The Welding Institute, London, U K, 1962; 123—132.

[2] Budai P. Measurement of droplet transfer stability in weld process with short circuiting drop transfer[J] . Conf. Computer Technology in Welding 1988, 13(6): 149—155.

[3] Gupta S R, Gupta P C. Effect of some variables on spatter loss[J] . Welding and Metal Fabrication, 1984, 54(11/ 12): 361—364.

[4] 安藤, 长谷川, 丰原. 裸电极棒使用の溶接电弧における短路の二形态[J] . 溶协志, 194, 10: 425—429.

[5] Amson L C. Analysis of the gas shielded consumable metal arc welding system. [J] . British Journal, 1962, 41(4): 232—249.

tion characteristics of AZ91D magnesium alloy rapid solidification ribbons[J] . Journal of Materials Science and Technology, 2004, 20 (4): 431—434.

[6] Wilson R D. Explore the potential of capacitor discharge welding[J] . Advanced Material Processes, 1994, 145: 93—94.

[7] Cavaliere P, Panella F. Mechanical and microstructural behaviour of CMSX—4 Ni—based superalloy joined by capacitor discharge welding [J] . Journal of Materials Processing Technology, 2007, 183: 297—300.

[8] Jianzhong Chen, Dave F, Farson Kevin Ely, *et al.* Modeling small—scale resistance spot welding machine dynamics for process control [J] . J Adv Manuf Technol, 2006, 27: 672—676.

[9] Feulvarch E, Robin V, Bergheau J M. Resistance spot welding simulation: a general finite element formulation of electrothermal contact conditions[J] . Journal of Materials Processing Technology, 2004, 153—154: 436—441.

[10] Chang B H, Zhou Y. Numerical study on the effect of electrode force

in small—scale resistance spot welding[J] . Journal of Materials Processing Technology, 2003, 139: 635—641.

[11] Matsugi K, Konishi M, Yanagisawa O, *et al.* Joining of spheroidal graphite cast iron to stainless steel by impact-electric current discharge joining[J] . Material Processing Technological, 2004, 150: 300—308.

[12] Carver M B, Salcudean M. Two-fluid modeling of phase redistribution by abstractions [J] . Mathematics and Computers in Simulation, 1987, 29: 399—412.

[13] Eric A Brands. Smithells metals references book [M] . London: Boston Butterworths, 1983.

作者简介: 翟秋亚, 女, 1963 年出生, 副教授, 硕士。主要从事先进材料及其焊接方面的研究。发表论文 40 余篇。

Email: xu—zhai @xaut. edu. cn

[上接第 46 页]

[6] Lancaster J F. The physics of welding. 2nd. ed[M] . Pergamon Press for the International Institute of Welding, 1985.

[7] Joo T M. Analysis of molten tip shape by energy method in GMA process[D] . MS Thesis. Korea Advanced Institute of Science and Technology (KAIST), 1994.

[8] Haider J, Lowke J J. Predictions of metal droplet formation in arc

welding[J] . Journal of Physics D: Applied Physics 1996 29 : 2951—2960.

作者简介: 王广伟, 男, 1980 年出生, 博士研究生。研究方向为图像处理, 短路过渡机理研究。发表论文 3 篇。

Email: Ryan. dre. king @gmail. com

es on A— TIG welding of magnesium alloy MA Xiang^{1,2}, ZHANG Zhaodong¹, LIU Liming¹, LIU Jinghe²(1. State Key Laboratory of Materials Modification & School of Materials Science and Engineering, Dalian University of Science and Engineering, Dalian 116024, China; 2. The Ministry of Education Research Center of Photo-Electricity Information Transmit of Materials & School of Materials Science and Engineering, Changchun University of Science and Technology, Changchun 130022, China). p39— 42

Abstract: For AZ31B magnesium alloy materials five kinds of single oxides MgO, Cr₂O₃, CaO, TiO₂, MnO₂ were used as the activating fluxes. The welding penetration, microstructures, phase composition and mechanical properties of welded joints without and with single oxide TiO₂ and the composite oxide were compared. The results of experiments showed that welding penetration of compound fluxes is 2.5 times than conventional tungsten inert-gas welding, also deeper than that with single flux. The crystal grain of the composite fluxes is smaller than that of single TiO₂ flux, and the tensile strength of the composite fluxes sample is superior to single TiO₂ flux sample. The activating element was added into weld that improve the phase composition of compound fluxes, which avoid the formation of the low-melting point magnesium-aluminum phase in the welded joint.

Key words: magnesium alloy; activating fluxes; unifom design method

Instantaneous short circuit in short circuiting transfer process in GMAW WANG Guangwei; CAI Yan; HUA Xueming; WU Yixiong (School of Materials Science and Engineering, Shanghai Jiaotong University; Shanghai 200030; China). p43 — 46, 102

Abstract: The critical condition of dynamic force equilibrium of instantaneous short circuit (ISC) in GMAW(gas metal arc welding) based on droplet pressure, electromagnetic force, and surface tension was presented while the dynamic force was analyzed. Based on micro focus high speed photography technique and digital image processing technology, the data of the droplet radius were obtained. And the electric signal was combined and analyzed. The results showed the short circuiting process reflects by the calculated data completely agreed with that from the images. The critical condition is proved. Further, the influence of the droplet shape on the ISC was analyzed based on this critical condition. If the radial radius was less than axial radius when the droplet touched with the wolten pool, the radial surface tension would be positive. The ISC stantes and can not be reversed, which means the spindly droplet leads to ISC frequently. Lastly, the ISC phenomena was classified and studied quantitatively. And the new explanation of ISC was proposed.

Key words: dynamic force equilibrium; instantaneous short circuit; gas metal arc welding

Dynamic monitoring of weld pod image for pulsed GTAW in welding scene WANG Zhijiang, ZHANG Guangjun, GAO

Hongming, WU Lin (National Key Laboratory of Advanced Welding Production Technology, Harbin Institute of Technology, Harbin 150001, China). p47— 50

Abstract Information on stability and continuity of welding process can be obtained by dynamic monitoring of weld pool. The dynamic monitoring of weld pool is still in laboratory stage. To monitor weld pool in the welding scene is more valuable in both welding process improvement and production guide. However, there are some problems in welding scene, for example, the welding power sources cannot be modified and incontrollable by personal computer; the waveforms of welding current and voltage are unknown and so on. For these problems, a weld pool image dynamic monitoring system was setup in the welding scene. According to the characteristics of pulsed GTAW(gas tungsten arc welding) in the welding scene, the time to take image, which is the most important factor to restrict to take image in the welding scene, is determined by external synchronization; using the spectral analysis, a compound filter system, which reduces the interference of arc, was proposed; at the optimum image taking hour, clear images of weld pool were obtained by CCD with the compound filter system in the welding scene.

Key words: weld pool; visual monitoring; pulsed gas tungsten arc welding; welding scene; spectral analysis

Effect of multi-passes welding on microstructure and properties of austenitic/ pearlitic dissimilar steel clad pipe SMAW welded joint WANG Nengli¹, ZHANG Xiyun¹, PAN Xide², XUE Jin² (1. School of Materials Science & Engineering, Changchun University of Science and Technology, Changchun 130022, China; 2. School of Materials Science & Engineering, Xi'an Jiaotong University, Xi'an 710049, China). p51— 54

Abstract Microstructures of transition weld and melted zone has the important effects on properties of austenitic/ pearlitic dissimilar steel clad pipe welded joint. Single-pass and multi-passes welded joints of 0Cr18Ni9/20 clad pipe were prepared by the use of shielded metal arc welding (SMAW) and E309L super-low carbon austenitic stainless steel electrode. Studies on the welded joint were made by means of optical metaloscopy, energy dispersive spectrum, scanning electron microscope, X-ray diffraction and microhardness analysis. The results indicated that re-heating of cover pass weld can decrease the size and the content of δ-ferrite in transition weld, and the morphology of δ-ferrite in transition weld turns from the vermicular type to the granular type. The chemical compositions of melted zone between transition weld and 0Cr18Ni9 base metal become more uniform. And there was no precipitation of Cr₂₃C₆ carbides in transition weld after re-heating.

Key words: multi-passes welding; clad pipe; super-low carbon austenitic stainless steel electrode; shielded metal arc welding

Control model and software flow of main circuit for 3— phase low frequency welder MA Tiejun, ZHANG Yong, LI Jinglong,